PROPERTIES OF PULSE ELECTRODEPOSITED $CuIn_XAl_{1-X}Se_2$ (X = 0.1, 0.2, 0.3) FILMS

M. THIRUMOORTHY[a*], K. RAMESH[b], K. R. MURALI[c]
[a]*Department of Physics, Bannari Amman Institute of Technology, Sathyamangalam, India*
[b]*Department of Physics, Government Arts College, C-Mutlur, Chidambaram, India*
[c]*Department of Theoretical Physics, University of Madras, Chennai, India*

In this present work, the pulse electrodeposition technique has been employed for the first time to deposit CIAS films. AR grade $Al_2(SO_4)_3$, $In_2(SO_4)_3$, 0.02 M $CuSO_4$, 0.05 M SeO_2 were used for the deposition. The films were deposited at 80°C and at different duty cycles at a constant current density of 5mA cm^{-2}.The concentration of $Al_2(SO_4)_3$ and $In_2(SO_4)_3$ were varied to obtain $CuIn_xAl_{1-x}Se_2$ films of composition (x = 0.1 to 0.3). X-ray diffraction studies indicated the films to exhibit single phase chalcopyrite structure. Optical transmission spectra exhibited interference fringes which was used to estimate the refractive index. Tauc's plot was used to estimate the band gap. The band gap was 1,15 eV, 1.29 eV and 1.43 eV respectively for the films with x = 0.1, 0.2 and 0.3. The optical dispersion parameters were determined. Photoelectrochemical cell studies were made on the films using 1M polysulphide electrolyte.

(Received September 7, 2017; Accepted November 6, 2017)

*Keywords:*Thin films, Semiconductor, chalcopyrite structure, I –III-VI_2, solar cell

1. Introduction

There has been increased interest in the I–III–VI ternary and quaternary semiconductors owing to their possible applications such as solar cells, parametric oscillators, nonlinear optical devices and detectors [1]. Among these materials, copper indium selenide ($CuInSe_2$) thin films are promising candidate for low cost solar cells. To increase the band gap Ga can be substituted for In and S for Se. This is likely to enhance the photovoltaic conversion efficiency in CuInSe based solar cells. Thin films of $CuIn_xGa_{1-x}Se_2$ showed an efficiency of 21% [2] after several years of continued research. However, gallium is a scarce and expensive material. $CuIn_{1-x}Al_xSe_2$ (CIAS) is a viable alternative material for the fabrication of heterojunction solar cells with low-cost and tandem cells [3]. By gradually substituting indium with aluminium, the optical band gap can be varied from 1.04 to 2.67 eV. In view of the above, attention has been devoted to the preparation of CIAS thin films by different methods such as the sequential deposition method followed by annealing/selenization [4,5], Coevaporation [6,7], flash evaporation [8], chemical bath deposition [9], and molecular beam epitaxy [10]. In this work, the pulse electrodeposition technique has been effectively employed for the first time to deposit CIAS films with x varying from 0.1 – 0.3.

2. Experimental

CIAS thin films were deposited by the pulse electrodeposition technique using ethylene glycol solution. AR grade $Al_2(SO_4)_3$, $In_2(SO_4)_3$, 0.02 M $CuSO_4$, 0.05 M SeO_2. The concentration of aluminium sulphate and indium sulphate was varied as follows, 2.o mM, 18 mM; 4 mM, 16 mM; 6

---

[*] Corresponding author: thirumoorthy@bitsathy.ac.in

mM, 14 mM respectively. Tin oxide coated glass (5 ohms/sq) were used as substrates. The films were deposited at 80°C and at different duty cycles at a constant current density of 5mAcm^{-2}. Thickness of the films measured using Mitutoyo surface profilometer was 700 nm, 785 nm and 825 nm with increase of aluminium (x) value increased from 0.1 – 0.3. The films were characterized by x-ray diffraction studies, optical absorption and photoelectrochemical studies.

2. Results and discussion

The X-ray diffraction pattern of CIAS films formed at different duty cycles is shown in Figure 1 (a) to Figure 1 (c). The films were polycrystalline exhibiting the peaks corresponding to (112), (220), (204), (312) and (116) orientations of the chalcopyrite structure as similar to earlier reports [11]. The crystallite size was calculated from the Full width half maximum of the diffraction by using Debye Scherrer's equation

$$D = \frac{K\lambda}{\beta cos\theta} \quad (1)$$

The crystallite size increased from 15 nm – 39 nm as the Indium concentration increased. The thickness of the films and crystallite size are shown in Table.1. The dislocation density δ, is the length of dislocation lines per unit volume of the crystal has been evaluated using the following equation

$$\delta = 1/D^2 \quad (2)$$

The length of dislocation lines per unit volume determine the dislocation density δ, of the crystal and it has been calculated using the following formula '[11].

$$\beta cos\theta/\lambda = 1/D + \varepsilon sin\theta/\lambda \quad (3)$$

The dislocation density is also presented in Table 1. From the table it is observed that, increase of grain size, the dislocation density will decreases. By using full-width at half-maximum 'β' of the diffracted peaks the strain 'ε' and particle size 'D' for the films was calculated through the following equation

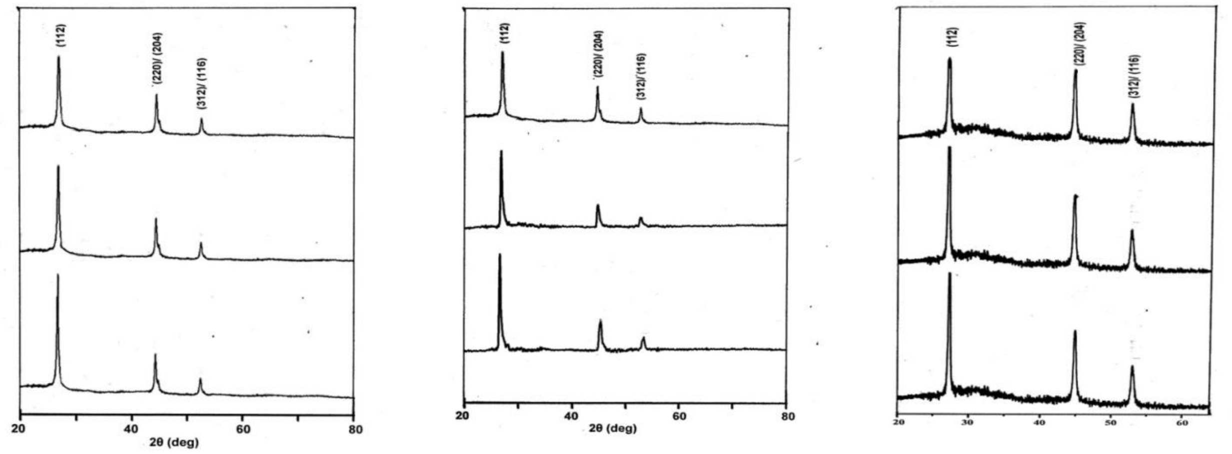

(a) x = 0.1 (b) x = 0.2 (c) x = 0.3

Figs. 1 (a) to (c) show the XRD patterns of $CuIn_{1-x}Al_xSe_2$ *films deposited at different duty cycle*

The plot of βcosθ/λ versus sinθ/λ allows us to find out both strain and particle size from slope and intercept of the graph. The measured values for thin films deposited at different duty cycle are listed in Table.1. The deviation in the bulk observed value and lattice parameter values are clearly suggest that the crystalline grains in the thin films are under stress. This behaviour is mainly due to deposition condition, change of nature and concentration of the local imperfections created in thin films. This leads to elongate or compress the lattice and slight change in structural parameters.

Table 1 Lattice parameters of $CuIn_{1-x}Al_xSe_2$ films with increase of Aluminum content

Al content (x)	**a (Å)**	**c (Å)**	**Thickness (nm)**	**Crystallite size (nm)**	**Strain ($x10^{-4}$)**	**Dislocation density ($lines/m^2x10^{15}$)**
0.1	5.747	11.501	1100	39	0.71	0.66
0.2	5.740	11.440	1034	37	0.76	0.73
0.3	5.712	11.379	987	34	0.82	0.87

Chemical composition of films was confirmed by energy dispersive analysis of X-ray technique (EDAX). Figure 2 shows the EDAX spectra of the$CuIn_{1-x}Al_xSe_2$ films of different composition. The peaks corresponding to Cu, In, Al and Se are observed in all cases. The composition of the films is shown in Table.2

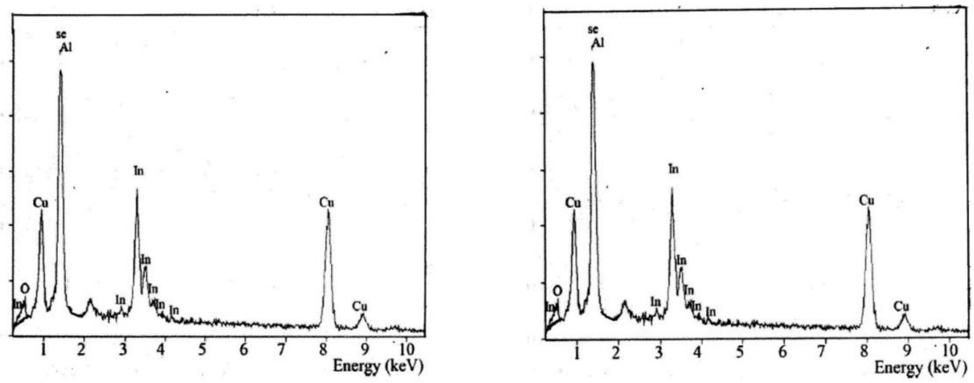

(a) X = 0.1

(b) x = 0.3

Fig.2. EDAX spectra of $CuIn_{1-x}Al_xSe_2$ films deposited at different duty cycle

Table2.Composition of $CuIn_{1-x}Al_xSe_2$of different composition deposited at 50 % duty cycle

Composition	Atomic percentage (%)				Cu/(Al+In)	Δm	Δs
(x)	Cu	In	Al	Se			
0.1	23.50	13.45	6.75	56.30	1.16	0.16	0.34
0.2	23.35	13.30	7.55	56.85	1.12	0.12	0.31
0.3	23.00	13.25	7.75	56.30	1.09	0.09	0.29

Fig. 3 shows the transmittance spectra of the $CuIn_{1-x}Al_xSe_2$films of different composition deposited at 50 % duty cycle. The value of the refractive index was estimated by the envelope method [12] The value of the refractive index, calculated from the above was in the range of 2.70 - 2.73 for the samples of different composition deposited at 50% duty cycle.

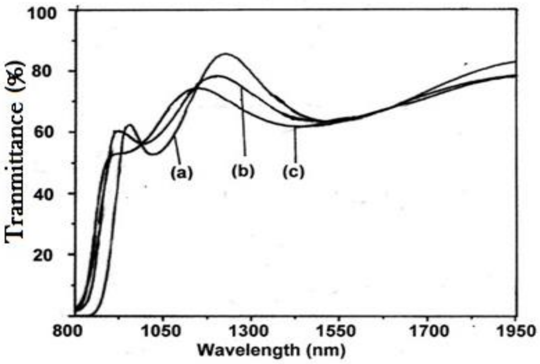

Fig.3.-Transmittance spectra of $CuIn_{1-x}Al_xSe_2$ films of different composition
(a) x = 0.3 (b) x = 0.2 (c) x = 0.1

A plot of $(\alpha h\nu)^2$ against hν, as indicated in Figs. 6.8 and Fig. 4, exhibited linear behavior near the band edge, the band gap of the deposited material wasdetermined to be in the range of 1.15 – 2.31 eV.

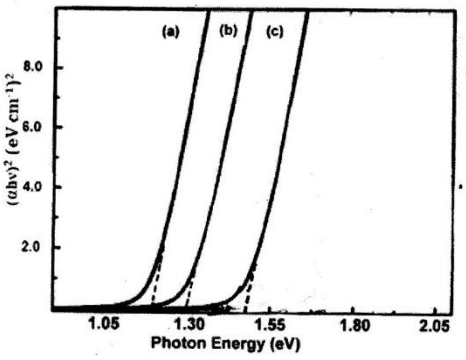

Fig. 4.Tauc's plot of $CuIn_{1-x}Al_xSe_2$ films of different composition
(a) x = 0.1(b) x = 0.2 (c) x = 0.3

According to Wemple and DiDomenico, the single-effective oscillator model is proposed from the following equation

Figure 5 shows that the films deposited at different composition at 50% duty cycle the graph plot between $(n^2 – 1)^{-1}$ Vs E^2 oscillator parameters fitting at a straight line the values of E_0 and E_d then calculate the slope $(E_0E_d)^{-1}$ and intercept on the vertical axis yields (E_0/E_d). From Wemple – Didomenico dispersion equation to $E\rightarrow0$ the static refractive index (n_0) is calculated. The values of n_0 are 2.775, 2.785, 2.81 and 2.83 for the films deposited at different composition at 50% duty cycle. The calculated values of E_0, E_d and n_0 are listed in table 3. In addition, the optical band gap (E_g) determined from the Wemple–DiDomenico dispersion parameter E_0 using the relation $E_g= E_0/2$, are also in good agreement with the band gap values determined from the $(\alpha h\nu)^2$ vs hν plot.

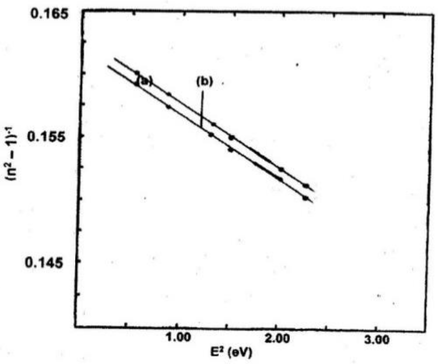

Fig. 5.Variation of $(n^2 - 1)^{-1}$ *with* E^2 *of* $CuIn_{1-x}Al_xSe_2$ *films of different composition (a) x = 0.1 (b) x = 0.3*

Table 3.Dispersion Energy values of $CuIn_{1-x}Al_xSe_2$ *films of different composition deposited at 50 % duty cycle*

Composition(x)	n_o	E_o	E_d (eV)	E_g (eV)
0.1	2.695	1.61	10.29	1.15
0.3	2.72	2.02	12.65	1.44

Photoelectrochemical (PEC) cells were prepared using the films of different composition deposited on titanium substrates. Due to redox electrolyte, the films metal substrate portion are exposed and is prevented by lacquered with polystyrene. These films are used as working electrode. PEC cell measurements were made by using the redox electrolyte as 1 M polysulphide (1 M S, 1 M Na_2S and 1 M NaOH). Here the counter electrode as Graphite. The Tungsten halogen lamp (ORIEL 250 W) is used as light source. To cut off the Infrared portion, the water filter was kept in between PEC cell and light source. The CEL suramapi is used to measure intensity of light falling on PEC cells and is calibrated in $mWcm^{-2}$. The intensity of light source falling on the PEC cells can be varied by changing the distance between the light source and PEC coil. By connecting an ammeter and the resistance box in series the power output characteristics of the PEC cells are measured and by connecting the load resistance across the PEC cell the voltage output measurements are taken by using the HIL digital multimeter.

The $CuIn_{1-x}Al_xSe_2$ photoelectrodes are dipped into the electrolytic solution for about 10 minutes under dark conditions and the value of dark current and dark voltage is noted. By varying the resistance in the resistance box when the cells are illuminated by the tungsten halogen lamp, the current and voltage are measured. The photovoltage and photocurrent were calculated as the difference between light under illumination for voltage and dark voltage, current under light illumination and dark current respectively.

The power output characteristics were obtained for the PEC cells made using the photo electrodes of different composition is shown in Figure 6. As observed from the figures the films have exhibited weak photoactivity, hence in order to increase photoactivity they were heat-treated at different temperatures in the range of 450 - 550ºC in argon atmosphere for 10 min. Further it is also observed that the films of composition $CuIn_{1-x}Al_xSe_2$ have exhibited high photooutput hence, further studies were made on the films of this composition. It was observed that the maximum PEC output for electrodes heated at 525°C irrespective of composition and hence the load characteristics were obtained for these electrodes. Figure 7 shows the load characteristics of the films of different composition, post heat treated at different temperatures.Photoelectrodes heat-treated beyond 550°C exhibited lower $V_{oc}$and J_{sc} values due to reduction in thickness. Amongst the electrodes of different compositions, electrodes with the composition $CuIn_{0.7}Al_{0.3}Se_2$ have exhibited the maximumV_{oc} of 0.67 V for 80 mWcm^{-2} illumination. At intensity values beyond 80mWcm^{-2},V_{oc} was found to saturate as is commonly observed for photovoltaic and PEC cells, $J_{sc}$was found to increase with increase in intensity of illumination. The effect of photoetching on the PEC performance was studied by shorting the photoelectrode and the graphite counter electrode under an illumination of 100 mW cm^{-2} in 1: 100 HCl for different durations in the range 0 – 100s. Both the photocurrent and photovoltage are found to increase upto 70s photoetch, beyond which they begin to decrease. Photoetching leads to selective attack of surface defects not accessible to chemical etchants**.** It is observed that during photoetching the V_{oc} increased from 0.67 V to 0.75 V and J_{sc} increased from 13.50 mAcm^{-2} to 21.00 mAcm^{-2}.The decrease in photocurrent and photovoltage beyond 70s photoetching can be attributed to increase in surface area due to prolongedphotoetching [13]. The power output characteristics (Figure 8) after 70s photoetching indicates a V_{oc} of 0.75 V, J_{sc} of 21.00 mA cm^{-2}, ff of 0.62, η of 12.21% for 60 mW cm^{-2} illumination. The photovoltaic parameters of the electrodes of different composition are shown in Table.4.

Photoetching process successfully decreases the density of recombination centers by etching out surface steps and imperfections. This leads to improvement in photocurrent the maximum observed increase in photocurrent was by more than three times and hence conversion efficiencies. It was found that surface steps, inhomogenities and defects are etched/removed as a result of photoetching. The photoetching process has been generally found to result in aslight increase in the photovoltage (open circuit voltage). This has been found to be a consequence of the change in flat band potential.

The density of recombination centers are decreased during photoetching process due to etching out surface steps and imperfections. This leads to improvement in photocurrent.

Photocurrent conversion efficiencies were increased by more than three times after photoetching. It is due to inhomogenities and defects are etched/removed in surface steps, the photoetching process has been generally found to increase the photovoltage (V_{oc}). This has been found to be a significance of the change in flat band potential V_{fb}. Photoetching is seems that one of the most capable surface treatment processes for improvement of conversion efficiency through containment of recombinations. The fill factor (FF) is another important Photo electrochemical Cell parameter which determines the solar to electrical energy conversion efficiency of the cell. It reflects the capability of photogenerated current to execute work through an external load and is therefore very responsive in the semiconductor/electrolyte interface to the kinetics of flow of current. In addition to photocurrent, the fill factor gets enhanced, but it has a lesser degree as a result of photoetching. The main reason is the recombination velocity of minority carriers to be decreases. Thus after the photoetching semiconductor/electrolyte interface behaves nearer to the ideal case this is the fact that the improvement in fill factor, i.e., the dark saturation current decreases (series resistance decreases), (shunt resistance increases). A side result of photoetching, there is formations of micro etch pits on the electrodes and also a roughening of the surface steps so there is a decrease in reflectivity and increase in absorptive of light that leads to better conversion efficiency. Similar performance was observed in WSe2 photoelectrodes [14].

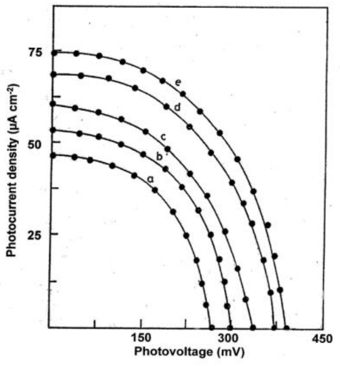

Fig. 6.Load characteristics of CuIn$_{1-x}$Al$_x$Se$_2$ films of different composition deposited at 50 % duty cycle (a) x = 0.1 (b) x = 0.3

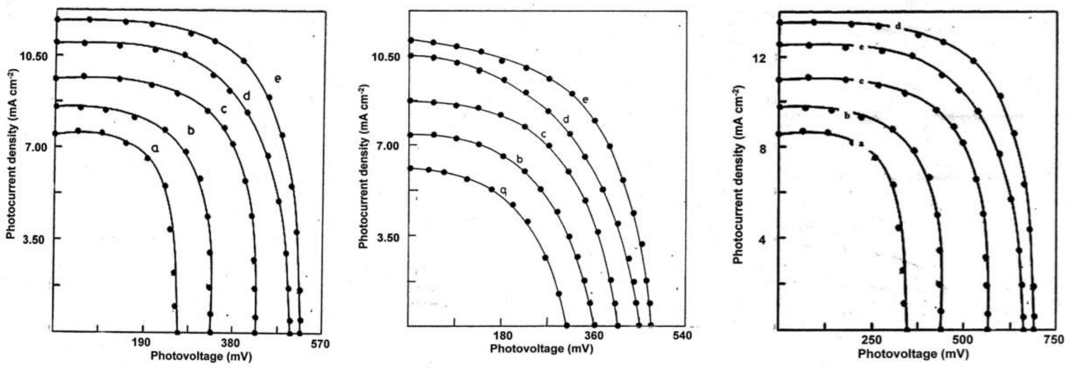

(a) x = 0.1 (b) x = 0.2 (c) x = 0.3

Fig. 7.Load characteristics of $CuIn_{1-x}Al_xSe_2$ films deposited at 50 % duty cycle post heat treated at different temperature (a) 450°C (b) 475°C (c) 500°C (d) 550°C (e) 525°C

\

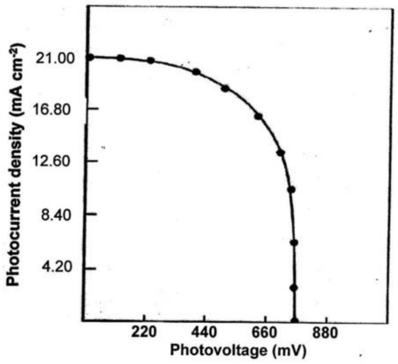

Fig.8. Load characteristics of $CuIn_{0.7}Al_{0.3}Se_2$ films deposited at 50% duty cycle and post heat treated at 525°C after photoetching for 80 s

Table 4.Photovoltaic parameters of $CuIn_{1-x}Al_xSe_2$ films of different composition deposited at 50 % duty cycle and post heat treated at 525°C(Intensity of illumination – 80mWcm^{-2})

Composition(x)	V_{oc}(V)	J_{sc}(mAcm^{-2})	ff	η (%)	R_s (Ω)	R_{sh}(kΩ)
0.1	0.55	12.0	0.72	5.94	12	2.00
0.2	0.46	11.0	0.61	3.85	14	1.90
0.3	0.67	13.5	0.68	7.69	9	2.20
0.3 (After photoetch)	0.75	21.0	0.62	12.21	5	2.10

3. Conclusions

Pulse electrodeposition technique have been used to prepare CIAS thin films. XRD analysis exhibit chalcopyrite structure. Composition of prepared films has been confirmed from EDS analysis. Slight excess of SE is present in all cases. Cu/(Al + In) ratio has been observed to be greater than unity in all cases. Optical transition has been found to be direct and allowed with the band gap of around 1.16–1.50 eV. Optical dispersion parameters were evaluated from the refractive index data. Oscillator energy is twice the band gap value. Photoelectrochemical cell studies indicated that films with composition $CuIn_{0.7}Al_{0.3}Se_2$ exhibited maximum efficiency of 12.21 % after photoetching.

References

[1] J.L. Shay, J.H. Wernick, Ternary Chalcopyrite Semiconductors: Growth, Electronic Properties and Applications, Pergamon Press, Oxford, (1975).

[2] P. Jackso, R. Wuerz, U. Rau, J. Mattheis, M. Kurth, T. Schloetzer, G. Bilger,J.H. Werner, Progress in Photovoltaics Research Application **15**, 507 (2007).

[3] Teodor K. Todorov, Douglas M. Bishop, Yun Seog Lee, Solar Energy Materials and Solar Cells, https://doi.org/10.1016/j.solmat.2017.07.033 (2017).

[4] Jae Ho Yun, R.B.V. Chalapathy, JeongChul Lee, Jin Soo Song, Kyung Hoon Yoon,Solid State Phenomena**124–126**, 975 (2007).

[5] J. Lpez-Garcia, C. Guillen, Thin. Solid.Film **517**, 2240 (2009).

[6] Y.Bharath Kumar Reddy, V. Sundara Raja, B. Sreedhar, Journal of Physics, Applied.Physics **39,**5124 (2006).

[7] S. Yamada, K. Tanaka, T. Minemoto, H. Takakura, Journal of Crystal Growth **311**, 731 (2009).

[8] K. Srinivas, J.N. Kumar, G.H. Chandra, S. Uthanna, Journal of Materials Science:Materials inElectronics **17**, 1035 (2006).

[9] B. Munir, R.A. Wibowo, Eun Soo Lee, Kyoo Ho Kim, J. Ceram., Journal of Ceramic Processing research **8**(4), 252 (2007).

[10] B. Kavitha, M. Dhanam, Materials Science and Engineering B **140**, 59 (2007).

[11] H. Mustafa, D. Hunter, A.K. Pradhan, U.N. Roy, Y. Cui, A. Burger, Thin solid films **515** (17), 7001 (2007).

[12] R. Swanepoel, Journal of Physics E: Scientific Instruments **16**, 1214 (1983).

[13] J.P. Mangalhara, R. Thangaraj, O.P. Agnihotri, Bulletin of Material Science **10**(4),333 (1988).

[14] I.H. Choi, P.Y. Yu, Journal of Applied Physics **93** (8), 4673 (2003).